Biomass Conversion and Biorefinery
https://doi.org/10.1007/s13399-022-03491-0

ORIGINAL ARTICLE

Silver adsorption on biochar produced from spent coffee grounds: validation by kinetic and isothermal modelling

Md Anwarul Islam[1] · Mst Irin Parvin[1] · Tewodros Kassa Dada[1] · Ravinder Kumar[1] · Elsa Antunes[1]

Received: 4 August 2022 / Revised: 23 October 2022 / Accepted: 24 October 2022

Abstract

This study investigates silver adsorption on biochar produced from pyrolysis of spent coffee grounds (SCGs). Biochars were produced from SCGs at temperatures between 500 and 1000 °C. SCG-derived biochars were then characterised by different analytical methods, such as Brunauer-Emmet-Teller (BET), Fourier transform infrared (FTIR), X-ray diffraction (XRD), and investigated for silver removal. The results revealed that the biochar produced at 500 °C offered a maximum surface area of 40.1 m^2/g with a yield of 23.48% biochar and the highest silver adsorption capacity of 49.0 mg/g with 99.9% silver removal efficiency. The morphology of adsorbed silver on biochar was determined using scanning electron microscopy–energy-dispersive spectrometry (SEM–EDS), and XRD analyses, which showed an even distribution of silver on the biochar surface. Furthermore, X-ray photoelectron spectroscopy (XPS) confirmed that part of the silver ions was reduced to form metallic silver (Ag^0)/silver nanoparticles (Ag NPs) during adsorption. The kinetics and isothermal evaluation suggested that silver adsorption was dominated by the pseudo-second-order model and Langmuir isotherm, which means that silver adsorption was mainly dominated by chemisorption and monolayer on biochar surface. Overall, this study suggests that 500 °C was the most feasible pyrolysis temperature to produce SCG-derived biochar with suitable physicochemical properties that can efficiently adsorb silver species from wastewater.

Keywords Pyrolysis kinetics · Biochar application · Adsorption kinetics · Spent coffee grounds · Silver pollution · Heavy metal removal

1 Introduction

Approximately 359 billion cubic metres of wastewater are produced each year around the globe, out of which only 63% of the wastewater is collected and 52% is properly treated, while 48% of the wastewater remains untreated and subsequently released into the environment [1]. Wastewater generated from domestic and industrial sources is generally contaminated with potentially toxic heavy metals such as lead (Pb), chromium (Cr), cadmium (Cd), mercury (Hg), silver (Ag), and other hazardous pollutants [2, 3]. Though several techniques are employed to remove the contaminants, including heavy metals, during the wastewater treatment process (WWTP), a major portion of heavy metals remains in the treated effluent that finally goes into the water bodies [4]. In addition, treated or untreated wastewater is widely used for agricultural and landscape irrigation [1]. Thus, heavy metal pollution becomes a serious threat to the global aquatic environment and human health [5, 6]. For instance, direct exposure to silver (Ag) can cause human health problems, such as liver and kidney disorders, eye and skin irritation, and chronic problems in the respiratory tract, and silver can also bio-accumulate in the food chain [7, 8]. The toxicity of silver (ions and nanoparticles) towards living cells, including human cells, has been demonstrated by several studies [9]. Therefore, to ensure the safety of human health and the ecosystem, it is highly important to treat the

Highlights
- Biochar produced at 500 °C exhibited the highest silver adsorption capacity.
- Silver adsorption was dominated by monolayer chemisorption.
- Strong affinity/interactions were observed between the adsorbent and adsorbate.
- XPS analysis confirmed the chemical transformation of silver ions during adsorption.

✉ Elsa Antunes
elsa.antunes1@jcu.edu.au

[1] College of Science and Engineering, James Cook University, Townsville, QLD 4811, Australia

Published online: 14 November 2022

wastewater to eliminate heavy metals like silver and other contaminants in wastewater prior to its further applications or final discharge [10, 11].

Several advanced technologies, such as the activated sludge process, sequencing batch reactor (SBR), ion exchange, and reverse osmosis, are available to eliminate silver from wastewater, but most of these technologies are considered highly expensive and inefficient to remove silver particles completely from the wastewater. In addition, current wastewater treatment facilities cannot completely remove silver due to its low concentration (μg/L level) and its toxic effect on the bacterium-dominant treatment process [12]. Adsorption has been gaining substantial interest for the efficient removal of silver from aqueous media, mainly because it is a simple, economical, and eco-friendly process [13]. Recently, many natural and synthetic adsorbents have been investigated for silver adsorption, for instance, activated carbons [14], clays [15], biowaste materials [16, 17], cellulosic materials [18, 19], zeolites [20], graphene [21, 22], and biochar [13, 23]. However, compared to other adsorbents, biochar has been demonstrated as a promising adsorbent for heavy metals because of its low production cost, negligible environmental footprint, and significantly high adsorption capacity [24].

Biochar can easily adsorb heavy metals [23]. The primary interactions between biochar and heavy metal adsorption constitute electrostatic interactions, ion exchange, precipitation, and chemisorption [13]. Biochar is known to contain a net negative charge and can bind to positively charged silver ions, thus could ultimately play a key role in silver adsorption [25]. Functional groups present on the biochar surface help the reduction of heavy metals. For example, a study confirmed that carboxyl groups in the biochar reduced Cr^{IV} into Cr^{III} [26]. In contrast, physicochemical properties of biochar such as pore size, particle size, surface area, and the number and type of functional groups affect the adsorption capacity of heavy metals. For instance, high surface area and porosity may provide additional sites and enhance the adsorption of silver species [25]. Numerous biomass-derived biochar applied to remove various heavy metals, such as arsenic (As), cadmium (Cd), lead (Pb), nickel (Ni), zinc (Zn), copper (Cu), chromium (Cr), antimony (Sb), and mercury (Hg) from wastewater [27].

Spent coffee grounds (SCGs) are the waste by-product of the coffee industry. Coffee grounds (CGs) are coffee beans that have been crushed to a powder. Coffee is prepared by forcing boiling water through the CGs. After the water has been forced through, what remains is SCGs. An average cafe in a large Australian metropolitan area in 2016 produced over three tonnes of SCGs (wet weight) per year, over 90% of which directly went to landfilling as SCGs do not have significant market value [28]. Landfilling of SCGs or any organic/food waste causes greenhouse gas emission that is a key concern for climate change through global warming [29]. A circular economy approach for SCGs will not only reduce the environmental impact by eliminating pollution from landfilling but also transform SCGs into value-added products.

Pyrolysis of SCGs is an environmentally sustainable process to convert waste into value-added resources [30], which could also be a potential route for safe disposal of about eight million tonnes of SCGs per year [31]. Optimisation of pyrolysis conditions, such as pyrolysis temperature, can improve the physicochemical properties of biochar to enhance adsorption capacity. Moreover, the bio-oil fraction can alleviate the pyrolysis energy cost and make the process economically more viable [32, 33].

Biochar produced from SCGs could be highly advantageous to support the circular economy of wastes and mitigate heavy metal pollution at the same time. Based on the literature review, only one investigation was found where SCG-derived biochar was used for silver removal in 2016 [34]. More research could open better possibilities for SCG waste disposal and mitigation of silver pollution. Therefore, we aimed to prepare biochar using SCGs as feedstock. SCGs were pyrolyzed at a wide range of temperatures between 500° and 1000 °C, biochar physicochemical properties were analysed, and the silver adsorption performance was investigated. A detailed adsorption kinetics evaluation and isothermal study of silver adsorption were also conducted to better understand the adsorption mechanisms.

2 Materials and methods

2.1 Materials

Wet SCGs were collected from Juliette's Espresso, a coffee shop at the JCU Townsville Bebegu Yumba campus, Queensland, Australia. SCG samples were dried in an oven at 105 °C overnight to remove residual moisture. Silver nitrate ($AgNO_3$), 99.99% wt/wt solid, was outsourced from Sigma-Aldrich (S6506-25G, lot#MKCJ2718).

2.2 Methods

2.2.1 Characterisation of SCG biomass wastes

The composition of biomass wastes plays a vital role in the final properties of biochar, particularly the textural properties like surface area and pore volume that enhance the adsorption of a contaminant. Therefore, proximate and ultimate analyses of SCG biomass were carried out to determine the percentage of moisture, volatiles, fixed carbon, ash content, elemental carbon (C), hydrogen (H), and nitrogen

(N) content. Oxygen (O) content was calculated from mass difference and considering the total mass of 100.

Ultimate or elemental analysis (EA) was done in a Costech Analytical Elemental Analyser 4010 (Valencia, CA, USA) fitted with a zero-blank auto-sampler. The analyser uses dumas combustion to form CO_2 and N_2 that are detected by a thermal conductivity detector (TCD). Standards were used to formulate a calibration curve from which the C and N percentages of the biomass sample were determined.

Thermogravimetric analysis (TGA) is an important technique to understand the thermal decomposition behaviour of a substance. The 'Discovery TA/SDT650' analyser was used for thermogravimetric analyses of SCG biomass samples. All thermal analyses were carried out in a nitrogen environment (N_2 flow rate, 50 ml/min) from 25 to 1000 °C with a heating rate of 10 °C/min. The TGA curves were obtained from the plot of a residual mass percent against temperature. The moisture content (%) and volatile matters (%) were calculated from the TGA curve. Moisture content (%) was calculated from the mass loss to 200 °C, and volatile matters (%) were calculated from the mass loss from 200 to 500 °C. To study pyrolysis kinetics, TGA and DTGA (derivative TGA) curves were further recorded at three different heating rates, 5, 10, and 15 °C/min. For each TGA analysis, about 20 mg of the SCG biomass sample was analysed.

Ash content was determined by heating around 10 g of SCG biomass sample (dry sample) at 600 °C for 6 h in a conventional furnace (air atmosphere). The sample was removed from the furnace (at room temperature) and cooled in a desiccator for an additional hour, then weighed. Ash content was calculated from Eq. 1:

$$Ash\ content(\%) = \frac{B - C}{A - C} \times 100\% \tag{1}$$

where B is the mass of the crucible plus the mass of biomass after heat treatment, A is the mass of the crucible plus the initial mass of the biomass, and C is the mass of the crucible.

Fixed carbon content (%) was calculated as below:

$$Fixed\ carbon\ content\ (\%) = 100\ \% - (Moisture\ \% + Volatiles\ \% + Ash\ \%) \tag{2}$$

2.2.2 Pyrolysis experiments and characterisation of biochar

Pyrolysis of SCG biomass was done in a nitrogen environment (N_2 flow rate, 3 L/min) using a fixed bed reactor and a conventional electrical tube (quartz) furnace–Termolab (Portugal). For each experiment, about 10 g of biomass waste was weighed in a quartz crucible and placed in the tube furnace. SCG biomass sample was pyrolysed at 500, 600, 700, 800, 900, and 1000 °C, with a heating rate of 10 °C/min and a residence time of 2 h to find the best pyrolysis temperature for SCG biochar production to be posterior used for silver adsorption. This wide temperature range was selected based on our previous studies and literature review. At least three pyrolysis experiments were performed for each pyrolysis condition. After each pyrolysis experiment, biochar was weighed, grounded, and collected for characterisation and adsorption testing.

Biochar yield (%) was calculated after each pyrolysis by the following Eq. (3):

$$Biochar\ yield = \frac{BC}{DBW} \times 100 \tag{3}$$

where BC is the weight of dry biochar and BDW is the weight of dry SCG feedstock.

The pH of biochar often influences the pH of the adsorption media, which might impact the performance of the adsorbent. To determine the pH of each biochar sample, 0.5 g of biochar was mixed in 10 ml of double-distilled water and shaken in an ultrasonic bath for 90 min to ensure good contact between the biochar and water [35]. The pH was then measured and recorded by the Thermo Scientific (Model: Orion Star A215) pH metre with an Orion 8157BNUMD probe.

Specific surface area (Brunauer-Emmet-Teller, BET surface area) is a key property of any adsorbent material [36]. BET surface area, total volume, and pore size of pores were measured by an N_2 adsorption and desorption phenomena using the Quantachrome Autosorb iQ3 gas adsorption analyser. Approximately 0.2 g of biochar was used for each run, and all biochar samples were analysed at least twice. Prior to each analysis, the sample was firstly degassed under vacuum conditions overnight at room temperature and then at 250 °C for an hour. The BET model was used to calculate specific surface area and the BJH (Barrett-Joyner-Halenda) adsorption model for pore size and total pore volume.

A Fourier transform infrared (FTIR) is the equipment for identifying surface functional groups, which attribute the surface polarity or the surface charge for chemisorption [37]. A Thermo Science i7ATR- FTIR analyser was used to estimate chemical functional groups presented in different biochar samples. Prior to the experiment, biochar samples were manually grounded to improve the homogeneity and obtain a fine powder (less than 75 µm) for the chemical analysis. A small amount of powdered sample was placed on a diamond ATR sample holder, and a total of 64 scans were collected per sample between 500 and 4000 cm^{-1}.

X-ray diffraction (XRD) analysis was used to understand the structural arrangement, or the crystallinity of biochar

obtained after pyrolysis. The Bruker Phaser D2 X-ray Powder Diffractometer, Cu radiation, was used. XRD spectra were obtained from 5° to 65° with a scan step size of 0.02° and a time step of 1 s.

2.2.3 Silver adsorption capacity and silver removal efficiency of SCG biochar

To evaluate the silver adsorption capacity, 0.1 g of each biochar was added into 50 mL of 50 mg/L silver solution. Silver concentration in the aqueous solution was measured before and after adsorption by inductively coupled plasma–atomic emission spectroscopy (ICP-AES). An Agilent 5100 Varian Liberty Series II (Singapore) was used, and a series of silver standards were measured at a wavelength of 338.289 nm to calibrate the instrument. An independent silver standard solution was measured along with every batch of sample solution for quality control and quantification purposes. The silver adsorption capacity (Q_t in mg/g of biochar) at a given time t was calculated by Eq. (4):

$$Q_t = \frac{\left(C_0 - C_t\right) \times V}{m} \tag{4}$$

where C_0 (mg/L) is the initial concentration of the silver in the aqueous solution, C_t (mg/L) is the concentration after adsorption at time t, V (L) is the volume of the solution, and m (g) is the amount of biochar used. The silver removal percentage (%) was obtained by Eq. (5).

$$\%\ of\ silver\ removal = \frac{\left(C_0 - C_t\right)}{C_0} \times 100 \tag{5}$$

After silver adsorption, biochar was separated from the liquid phase using filter paper that was then dried at 105 °C overnight and analysed by XRD at room temperature. Scanning electron microscopy combined with energy-dispersive spectroscopy (SEM–EDS) was used to examine the microstructure and silver distribution on biochar before and after adsorption tests. A Jeol JSM5410LVA SEM was used for the analysis where a beam of high-energy electrons scanned across the surface of a sample to obtain high magnification and high-resolution images.

X-ray photoelectron spectroscopy (XPS) analysis was carried out to reveal the elemental composition and oxidation states of biochar surfaces and adsorbed silver. A Kratos Axis Supra connected with a monochromated Al Kα X-ray source and a helium lamp for UPS measurements were used. The binding energy was calibrated by the C 1 s peak at 284.6 eV. XPS peak processing software was used to deconvolute the peaks and identify different species of the same element.

3 Results and discussion

3.1 Characterisation of SCG biomass wastes

The results of ultimate and proximate analyses of SCG biomass samples are presented in Table S1. The ultimate analysis data indicate that SCGs contained a high percentage of elemental carbon (C) of 47.5% and fixed carbon of 18.8%. Both carbon content values obtained in this study were similar to the previous studies; for instance, elemental carbon and fixed carbon were reported at 18.58% and 43.68%, respectively, for rice straw [38]. In addition, SCGs had 71.5% of volatiles and a low oxygen (O) content, approximately 43.7%, which might be advantageous to produce the bio-oil with a high heating value [39]. On the other hand, the proximate analysis revealed that SCGs contain only 2.5% ash, indicating their suitability for biochar production via pyrolysis. Based on the ultimate and proximate analysis data, it can be suggested that SCGs might be a suitable biomass to produce biochar.

TGA and DTGA analyses in Figure S1 show the thermal decomposition behaviour of SCG biomass. TGA and DTGA curves can be separated into three stages, as shown in Table S2. Stage 1 (up to 200 °C) is mainly attributed to the loss of moisture and other volatile substances extractable from water. For instance, SCG biomass released a moisture content of 4.73%. Stage 2 is considered the main stage where the majority of the weight loss occurs, contributing to the depolymerisation of biomass components, such as hemicellulose, cellulose, and lignin. Hemicellulose is known to be completely depolymerised at 350 °C, while the degradation of cellulose starts above 180 °C and is completely degraded at 400 °C [29]. In contrast, depolymerisation of lignin polymers starts above 180 °C and is completely decomposed by 800 °C [40]. In stage 2, SCGs had a mass loss of 72.40%, corresponding to the temperature range of 200–550 °C. Similar results were reported in a previous study; a mass loss of 75% for SCGs was reported at this stage by Li et al. [29]. In addition, SCG mass loss of up to 330 °C was attributed to hemicellulose decomposition, and the last DTGA peak was found to be at 392 °C, which is associated with the decomposition of higher lignin and lipids [41]. The last stage, up to 800 °C, is attributed to solid decomposition, where the weight loss rate is slower, and a slight weight loss could be due to char consolidation [42]. For instance, the final stage weight loss for SCGs was 1.95%.

3.2 Kinetics analysis of biomass pyrolysis

3.2.1 Effect of heating rate

TGA and DTGA curves of SCGs were recorded at three different heating rates of 5, 10, and 15 °C/min. Figure 1a–b

shows the effect of heating rates on TGA and DTGA curves. The decomposition behaviour was similar at three different heating rates. It can be observed from Fig. 1b that the DTGA peaks reached the maximum value at 10 °C/min, and the DTGA curves shifted to a higher temperature zone when increasing the heating rate. These findings indicate the uneven heat transfer through the particles of SCG biomass. For instance, the temperature in the centre of the SCG particles is lower than the temperature on the surface [43]. The heat transfer efficiency was poor at a high heating rate compared to a low heating rate [44]. This heat transfer limitation and shifting of the DGTA curves towards the higher heating rate was also observed during the pyrolysis of coffee wastes and other biomasses in previous investigations [45].

3.2.2 Determination of activation energy

TGA and DTGA data at three different temperatures were used to derive the kinetic parameters using model-free methods, as shown in Fig. 1 (c–d). To calculate the iso-conversion plot of activation energy, E_α, with a degree of decomposition α, the degree of decomposition was considered up to 90% with a 10% size of each step according to the recommendation by the Kinetics Committee of the International Confederation for Thermal Analysis and Calorimetry (ICTAC) [46].

Activation energy, E_α, is the minimum energy that is required to initiate a chemical reaction. The high activation energy of a reaction means that this reaction requires a long residence time or high reaction temperature to start the reaction. Ozawa-Flynn-Wall (OFW) and Kissinger–Akahira–Sunose (KAS) methods were used to obtain kinetic plots; results are shown in Fig. 1 (c–d), and the calculation details are reported in Supplementary data (Table S8). The activation energy for SCGs using the OFW method varied from 143.80 to 269.74 kJ.mol^{-1} with an average of 188.59 kJ.mol^{-1}, and by the KAS method varied from 142.69 to 271.98 kJ.mol^{-1} with an average of 188.38 kJ.mol^{-1}. In this study, the average values of activation energy calculated by both the OFW and the KAS methods were similar to previous studies where the activation energy values were 196.08 and 197.26 kJ.mol^{-1} for SCGs from OFW and KAS methods [47]. Overall, all kinetic parameters calculated by the two methods were in good compliance with each other and could be used to simulate the decomposition process under a specific condition.

According to Figure S4, the required activation energy for the removal of extra moisture was low. A gradual increase of the activation energy up to 0.5 degrees of conversion was reported for the pyrolysis of SCGs. However, a slight decrease in activation energy from 0.5 to 0.7 degrees of conversion was noticed. This gradual increase suggests that SCG decomposition initiation requires high activation energy, and a slight decrease indicates the completion of the decomposition of cellulose and hemicellulose [48]. The

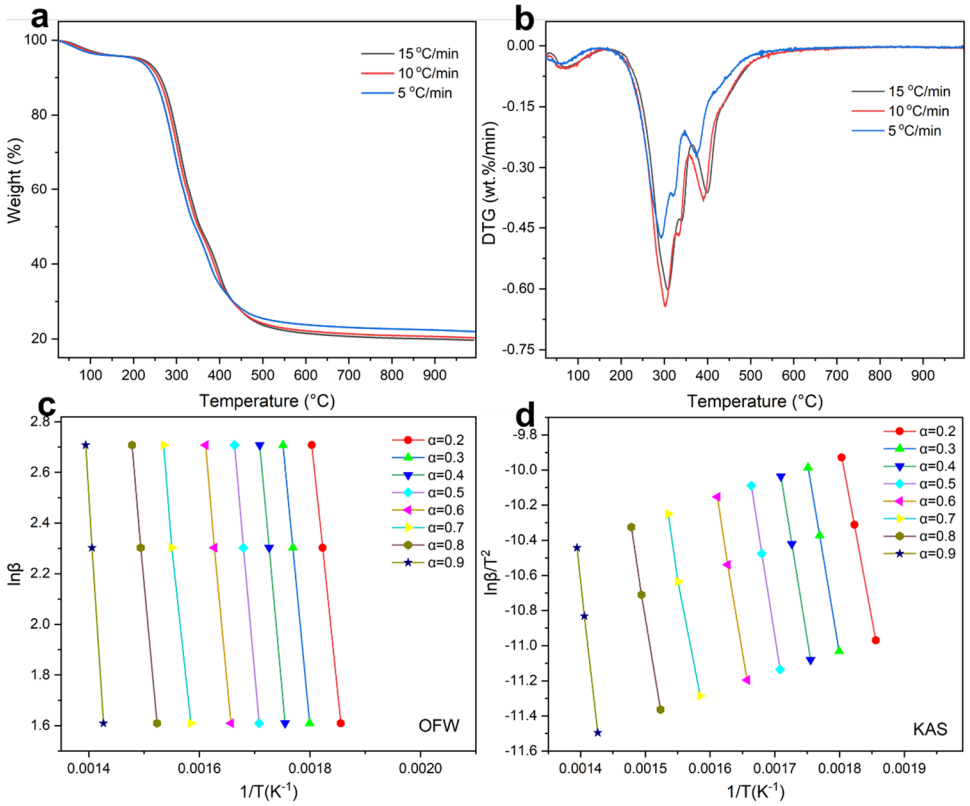

Fig. 1 **a**TGA and **b** DTGA curves of SCG biomass at heating rates of 5, 10, and 15 °C/min; **c** kinetic plots obtained from OFW and **d** KAS methods for SCGs

final stage, after 0.7 degree of conversion, required activation energy sharply increased to complete the decomposition of lignin which required extra energy [49].

3.3 Pyrolysis thermodynamics analysis

The apparent activation energies, E_α, calculated from the KAS method were used to derive the thermodynamic parameters, such as pre-exponential factor (A), the kinetic reaction rate constant, k, enthalpy (ΔH), entropy (ΔS), and the Gibbs free energy (ΔG) as shown in supplementary data (Table S9). Pre-exponential factor (A) values exhibited wide variations for a range of conversion degrees from 10^{15} to 10^{21}, which was attributed to the complex composition of SCGs as well as complex decomposition reactions during the thermal conversion. The low pre-exponential factors ($A < 10^9$ min^{-1}) also imply surface reaction, whereas the high pre-exponential factors ($A \geq 10^9$ min^{-1}) indicate the formation of the activated complex, which probably restricts rotation compared to the initial decomposition [50]. However, similar values of pre-exponential factors, 10^{19} to 10^{21}, were reported for the KAS method in previous studies [49].

The enthalpy changes (ΔH) demonstrate the energy difference between the reactant (biomass) and decomposition products [51]. Positive enthalpy indicates an endothermic reaction, while negative enthalpy indicates an exothermic reaction [52]. The enthalpy changes (ΔH) at various decomposition stages are presented in Table S9, with an average value of ΔH for SCGs being 183.29 kJ·mol^{-1}. It is important to note that Py-GCMS analysis (Figures S2 and S3, Tables S4 and S5) in this study and previous research showed that higher molecular weight compounds were identified in SCGs, and require higher energy to decompose [41]. In addition, a small difference (~5 kJ·mol^{-1}) in average activation energy derived from both methods was observed, which demonstrated that thermal decomposition is a favourable conversion process [53].

The Gibbs free energy changes (ΔG) are also presented in Table S9, and the average value is 133.15 kJ·mol^{-1}. The Gibbs free energy mainly indicates the total energy increase during the decomposition reactions [50], where a gradual increase of ΔG was reported with the degree of decomposition. High Gibbs free energy changes (ΔG) of coffee grounds were reported to be 173.09 kJ·mol^{-1} in a previous study [54]. This relatively high Gibbs free energy change indicates that the decomposition reactions consume significant energy, which makes the pyrolysis process thermodynamically unfavourable [52].

Entropy (ΔS) represents the degree of disorderness of the reaction system. The smaller value of ΔS indicates the system is near its thermodynamic equilibrium, which also suggests the system is less reactive. In contrast, a high value of ΔS suggests the higher reactivity of the system to form an activated complex [50]. According to Table S9, the average value of entropy was reported as 0.1 kJmol^{-1} K^{-1} which is similar to the previous study for bamboo biomass [52]. Positive values of ΔS in SCGs imply a high degree of disorderliness in the system after decomposition and formation of less stable pyrolysis products than the biomass [55].

3.4 Production and characterisation of SCG biochar

Table 1 shows SCG biochar yields and textural properties of the produced biochars at the studied temperatures of 500 to 1000 °C. Results revealed that increasing the temperature gradually decreased the biochar yield. The highest SCG conversion into biochar was observed at 500 °C pyrolysis, which produced 23.5% biochar, and the lowest was at 1000 °C, producing 21.8% biochar. However, the reduction in biochar yield from 500 to 1000 °C was not significant and was expected according to TGA analyses [56]. These results from our study are consistent with previous studies that demonstrated the decrease in biochar yield with an increase in temperature [57]. For instance, SCGs pyrolysed at 400 °C and 700 °C produced 43% and 26%, respectively [58]. Therefore, it could be suggested that lower pyrolysis temperature could be helpful to achieve higher biochar yield and could be comparatively more economical since less

Table 1 SCG-derived biochar yields at different pyrolysis temperatures and their physicochemical properties

Pyrolysis temperature (°C)	Elemental analysis (%)				Biochar yield (%)	pH	Surface area[a] (m^2/g)	Pore volume[b] (cc/g)	Pore size[c] (nm)	Silver adsorption capacity (mg/g)	Silver removal (%)
	C	H	N	O[x]							
500	70.50	2.87	3.69	22.94	23.48	10.29	40.10	0.019	3.28	49.00	99.90
600	75.82	2.89	4.63	16.66	22.74	10.40	31.30	0.012	5.18	47.30	96.00
700	76.29	2.61	3.23	17.87	22.14	11.02	33.50	0.013	6.01	48.40	99.70
800	77.73	1.16	3.26	17.85	22.33	10.38	5.20	0.003	8.14	28.70	57.70
900	80.08	0.87	3.83	15.22	21.86	11.27	3.40	0.005	16.04	25.30	51.50
1000	83.53	2.01	2.04	12.42	21.78	10.53	7.50	0.005	7.13	23.60	48.10

x = calculated by the difference; [a]BET surface area; [b]MP (micropore analysis proposed by Mikhail) method; [c]BJH (Barrett, Joyner & Halenda) method

energy would be used for pyrolysis. However, in addition to biochar yield, it is critical to obtain biochar with suitable textural properties, such as high surface area, pore volume, and physicochemical properties like high acidic functional groups to achieve high adsorption capacity.

Specific surface area (BET), pore volume, and pore size results of each SCG biochar sample are presented in Table 1. Specific surface areas of SCG biochar were reported as 40.1 to 3.4 m^2/g which are very low compared to other lignocellulosic origin-derived biochar, such as biochar produced from sugarcane bagasse and wood pyrolysed at 500 °C that reported surface area of 202 and 316 m^2/g, respectively [59], whereas SCGs pyrolysed at 500 °C previously reported only 1.46 m^2/g [31]. One of the reasons might be the smaller number of micropores in the biochar matrix. For instance, in this study, SCG biochar produced at 500° and 800 °C provided a pore volume of 0.019 and 0.003 cc/g, respectively, but BET surface area of 40.1 and 5.2 m^2/g, respectively. A maximum BET surface area of 40.1 m^2/g was found for the biochar produced at 500 °C, and the minimum was 3.4 m^2/g at 900 °C.

Additionally, biochar produced at 500 °C had a minimum pore size of 3.28 nm with a maximum pore volume of 0.019 cc/g. These results were significantly higher than in the previous study where the specific surface area and pore volume were 11.0 m^2/g and 0.009 cc/g, respectively, under the same pyrolysis conditions for SCG biochar [60]. The pore size increased with the increase in pyrolysis temperature. Biochar produced at 900 °C had the largest pore size of 16.04 nm diameter, providing the lowest surface area. This might result from collapsing of pores, which leads to the formation of larger pores, but at 1000 °C, these pores might shrink again. Pore size increased gradually till 900 °C, then again decreased to 7.13 nm at 1000 °C. These results indicate the weakness of the BET surface area measurement technique, such as the N_2 adsorption–desorption process, where complete desorption might not be able to be achieved and, consequently, is unable to accurately measure the surface area of SCG biochar. For instance, BET analysis of these biochars took a long time, and the results provided a non-linear BET curve and a non-equilibrium system of adsorption–desorption of N_2, which might be responsible for less accurate results [30]. Degassing the pore and high burn-off degrees or long residence time might be responsible for widening the micropores, thus providing low surface area [61]. In addition, the BET technique is not valid for macroporous materials, and SCG biochar might be one of these materials based on SEM images [62]. This observation was similar to the previous study which reported the inaccurate surface area from the BET method for the material having mesopores larger than 2 nm [63].

Elemental analysis results of SCG biochars produced at different temperatures between 500° and 1000 °C are summarised in Table 1. As expected, carbon content was found to increase with the pyrolysis temperature, while oxygen content decreased. The maximum carbon content of 83.53% was found in the biochar produced at 1000 °C, and the minimum carbon content of 70.5% was found in the biochar produced at 500 °C. In contrast, the oxygen content of 22.94% was the highest in biochar produced at 500 °C and the lowest at 12.42% in the biochar produced at 1000 °C. These findings demonstrated that oxygen-containing groups decomposed at high temperatures either in the form of pyrolytic gases like CO_2, CO, or NO_x and eventually decreased the oxygen content and increased the carbon proportion in the residual biochar [40]. Similar elemental composition of SCG biochar was observed in previous studies [61].

Table 1 presents the pH results of SCG biochar produced at various pyrolysis temperatures. Based on the experimental results, all SCG biochars were alkaline in nature as the pyrolysis process led to the formation of alkaline minerals from micronutrients in the biomass [64] with a slightly non-linear change with temperature. However, alkalinity was slightly increased with the increase in pyrolysis temperature, which indicates a decrease in acidic functional groups, such as – OH, and – COOH [65].

Peaks identified in FTIR spectra of different SCG biochar samples are summarised in Table S3. The results revealed that lower pyrolysis temperatures produced biochar with a larger number of functional groups, demonstrating the presence of a variety of organic compounds in the biochar. For example, biochar produced at 500 °C showed peaks at 1050, 1470, and 1890 cm^{-1}, which can be attributed to the presence of oxygen-containing alcoholic groups, aliphatic C – H groups, and aromatic C – H stretching, respectively. Conversely, increasing pyrolysis temperature started consistently decreasing the number of functional groups in the biochar, suggesting the volatilisation of organic compounds into pyrolytic gases and their condensation into the bio-oil. For instance, biochar formed at 600 °C showed peaks at 1470, 1900, and 2100 cm^{-1}, which can be ascribed to the occurrence of organic compounds with aliphatic C – H, aromatic C – H, and C≡C, respectively. In addition, a temperature of 1000 °C produced biochar with only aromatic compounds C – H. The analyses show that higher pyrolysis temperature enhances the decomposition of organic compounds into pyrolytic gases and bio-oil, leaving the biochar with a very few less or a negligible number of functional groups that are necessary for the adsorption of heavy metals. Therefore, lower pyrolysis temperatures should be applied for biochar production to generally result in a variety of functional groups in biochar, which could play a pivotal role as adsorption sites.

The XRD analysis spectra of different biochars produced under different pyrolysis temperatures are presented in Fig. 2a. XRD patterns showed nearly

amorphous structures of all biochars. The broad peaks at 2θ of 24.5° and 43° regions indicate amorphous carbonaceous structures. However, amorphous carbonaceous structures rearranged at higher temperatures to form a graphitic structure are characterised by broad peaks at 2θ of 24.5° [66].

3.5 Silver adsorption study by SCG biochar

The results of the silver adsorption performance of SCG-derived biochar are shown in Fig. 2c and Table 1, which revealed that biochar produced at 500 °C showed a maximum adsorption capacity of 49.0 mg/g and 99.9% silver removal performance. In contrast, biochar produced at 1000 °C provided the lowest adsorption capacity of 23.6 mg/g and 48.1% silver removal. In addition, SCG biochar produced at 600 and 700 °C provided the adsorption capacity of 47.3 mg/g and 48.4 mg/g with 96% and 99.7% silver removal, respectively. The decrease in adsorption capacity and % of silver removal with increasing pyrolysis temperatures can be attributed to textural properties, such as low surface area, pore volume, and less acidic groups in biochars. Since the biochars with a low surface area and negligible functional groups showed low adsorption capacity, it can be estimated that physisorption (that might include Van der Waal forces) played a major role in silver removal [67]. A previous study confirmed similar findings where high pyrolysis temperature (> 500 °C) reduced the functional groups of biochar and thereby the adsorption capacity for Cd reduced significantly [68]. On the other hand, biochars that contained a significant number of functional groups favoured the chemisorption mechanism for silver adsorption [69].

Table 2 presents the comparison of silver adsorption capacities by biochars derived from different biomass wastes. According to Table 2, the maximum silver adsorption capacity achieved was 137.4 mg/g with a 2000 mg/L of Ag^+ solution, which was high compared to other studies. This difference can be explained by the direct impact of initial high concentration and different types of biomasses [70]. However, for a similar initial concentration of Ag^+, SCGs in this study offered the highest adsorption capacity. Despite having a low specific surface area, the SCG biochar showed a higher adsorption capacity (49.0 mg/g after 24 h) than biochar produced from biosolids (43.9 mg/g), which had a higher specific surface area (38 to 151 m^2/g) [13]. Similarly, wood biochar having a specific surface area of 83.6 m^2/g provided the maximum silver adsorption capacity of 19.1 mg/g which was half of the SCG biochar [71]. This observation demonstrated that SCG biochar has substantial potential for Ag removal from aqueous waste mediums, mainly because of the presence of various oxygen-containing functional groups and other metals that participated in different Ag removal mechanisms.

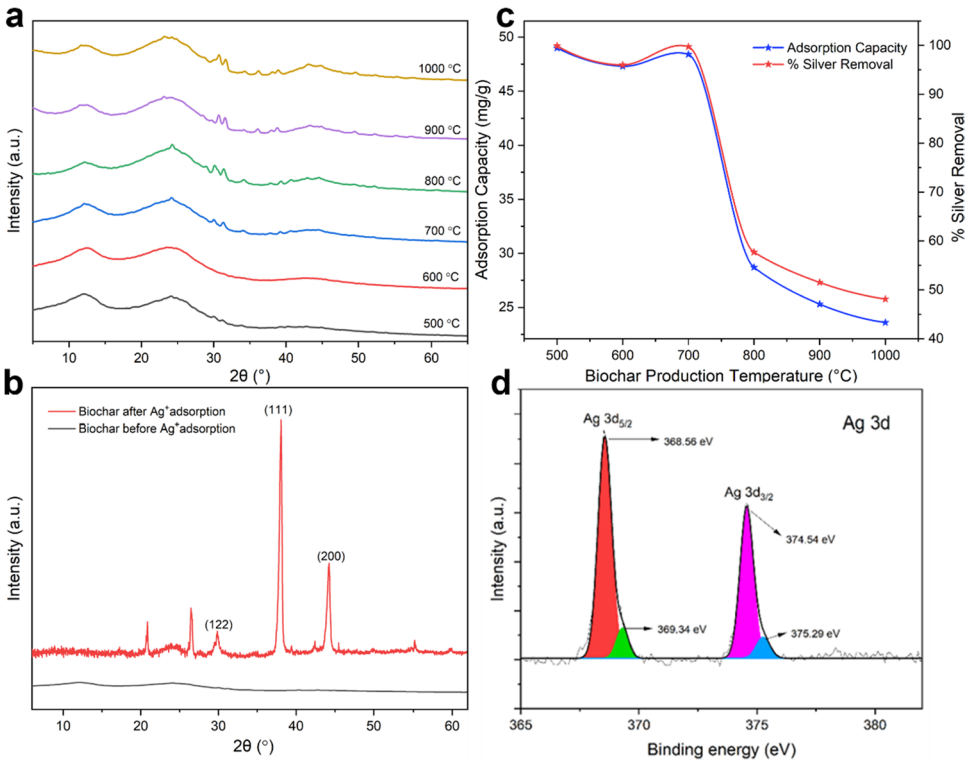

Fig. 2 **a** XRD spectra of SCG biochar obtained at pyrolysis temperatures from 500 to 1000 °C. **b** XRD analysis of SCG biochar (500 °C) before and after Ag^+ adsorption. **c** Silver adsorption capacity and removal % of SCG biochar after 5 h. **d** XPS analysis of biochar after silver adsorption

Table 2 Comparison of silver adsorption capacity of different biomass-derived biochars

Type of biomasses	Adsorption capacity (mg/g)	Initial silver concentration (mg/L)	Reference
Biofuel residue	90.06	50–100	[25]
Biosolids	43.9	100–1000	[13]
Sunflower husk Rapeseed Wood waste	22.9 26.9 19.1	100–300	[71]
Gracilaria R. algae	4.7	50–100	[72]
Pomelo peel	137.4	2000	[70]
Pine sawdust and bagasse	0.60–5.25	170	[73]
SCGs	46.2	50	[34]
SCGs	49.0	50	This study

3.6 Silver adsorption kinetics

The physical and chemical properties of the biochar can affect the adsorption behaviour of Ag. Kinetic studies can provide vital information to understand the physicochemical mechanism of silver adsorption on the SCG biochar, involving chemical binding and mass transport. Based on silver adsorption performance, biochar produced at 500 °C was selected and used to evaluate the kinetics and isothermal behaviour of silver adsorption from an aqueous solution. The adsorption capacity was measured by varying the contact time from 5 min to 24 h. Finally, the experimental data were compared with different kinetic models, such as pseudo-first-order (eq. S16), pseudo-second-order (eq. S17), intraparticle diffusion (Weber and Morris) (eq. S18), and the Elovich equation (eq. S19); results are shown in Fig. 3a and Table S6. The results suggest that the silver adsorption on the biochar surface occurred in two steps. For instance, the adsorption of silver ions was rapid at the beginning (up to 2 h contact time) and reached equilibrium after around 8 h. These findings demonstrate that silver ions were rapidly adsorbed by the adsorption sites on the outer surface of the biochar matrix, and after the first 2 h, silver ions diffused into the pores slowly. This second step could be explained by intraparticle diffusion, which reduced the adsorption rate. The results confirm the contribution of both chemical (slow) and physical (rapid) adsorption phenomena.

Compared to all kinetic models, the pseudo-second-order model fits well with the experimental data, having R^2 values of 0.9990, followed by the pseudo-first-order model (Table S6). Experimental data also showed that 61% silver was adsorbed in the initial 5 min. The fitting of results with the pseudo-second-order model suggests that the silver adsorption was mainly dominated by chemisorption, carried out by the functional groups and minerals present on the biochar surface, and physisorption that mainly involves the Van der Waals forces. Additionally, a low k_2 value of 0.0010 g/(mg h) indicated that the adsorption process was driven by the number of unoccupied sites in biochar [74]. The pseudo-second-order model also explained the additional complex mechanisms, such as surface adsorption, external liquid film diffusion, and precipitation [13]. Our results are consistent with previous studies that showed that biochar-driven heavy metal removal follows the pseudo-second-order and pseudo-first-order kinetic models. For example, a study carried out the application of sludge-based biochar for Pb(II) adsorption and showed that the adsorption kinetics followed the pseudo-second-order and pseudo-first-order models since the values of R^2 were greater than 0.99 [75]. In another study, biochar was applied for the adsorption of Ni(II) and Co(II) and the results revealed that both metals primarily followed the pseudo-second-order and then pseudo-first-order kinetics, suggesting the adsorption of Ni(II) and Co(II) was controlled by chemisorption process [76].

3.7 Silver adsorption isotherms

Adsorption isotherms were studied to understand the affinity between silver ions and biochar, and the results are shown in Fig. 3b and Table S7. The adsorption isotherms showed the

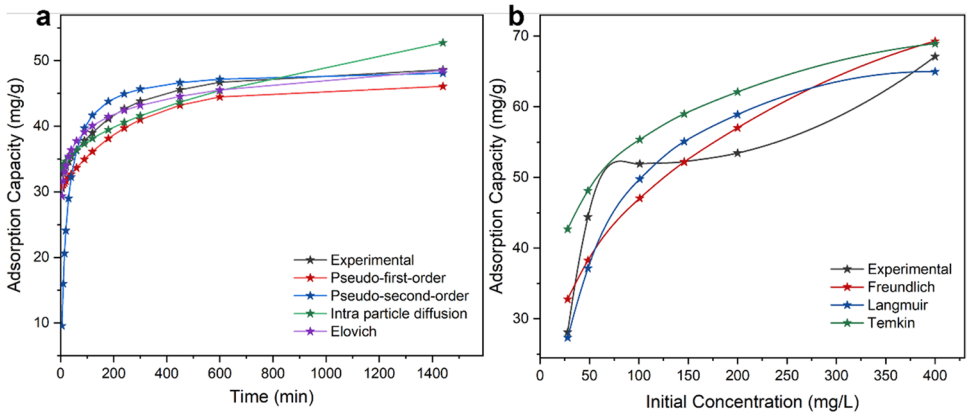

Fig. 3 **a** Silver adsorption kinetics by SCG biochar; **b** adsorption isotherms of silver adsorption by biochar, including experimental data and theoretical models

impact of the initial silver concentration in the solution on silver removal capacity by biochar under a constant pH and isothermal condition (22 ± 2 °C). The same biochar showed an adsorption capacity of 28.1 mg/g in 25 mg/L silver solution and 67.1 mg/g in 400 mg/L silver solution with the same retention time of 5 h. These findings indicate that higher concentration increases the driving force of mass transfer during the interaction between the solid and liquid phases and increases adsorption capacity [13].

The experimental data were compared with different isotherm models, such as the Langmuir model (eq. S20), Freundlich isotherm (eq. S21), and the Temkin isotherm (eqs. S24 and S25). The Freundlich model assumes mathematically unlimited adsorption sites on heterogeneous adsorption surfaces and the Langmuir model is an ideal monolayer adsorption model, assuming that all the adsorption sites have equivalent adsorption energies and there are no mutual interactions between adsorbed molecules [77]. Among all isothermal models, the Langmuir model fits the experimental data better, as the R^2 value of the Langmuir model was the highest at 0.987, whereas Freundlich and Temkin's models provided R^2 values of 0.8589 and 0.9131, respectively. Langmuir's model indicates monolayer adsorption of Ag on a homogeneous biochar surface, which is in line with the adsorption kinetic analysis. However, previous studies showed that the Langmuir model was also used to simulate the adsorption process by chemical precipitation [78]. In addition, the separation factor, R_L, indicates the nature of the adsorption process. Generally, $R_L > 1$ indicates unfavourable; $R_L < 1$ indicates favourable, $R_L = 1$ indicates linear; and $R_L = 0$ indicates irreversible adsorption phenomenon. In this study, R_L was 0.1031, which indicates that the adsorption was favourable; thus, the affinity or bond strength was strong between the adsorbate and adsorbent [31]. The strong affinity can be attributed to the high pore volume in the biochar that provided better accessibility and increase sorption sites for Ag species. In addition, the presence of oxygen-containing functional groups on the biochar surface is also responsible for enhanced affinity for Ag ions [79].

3.8 Characterisation of silver-loaded biochar

All biochar samples studied for silver adsorption were characterised by XRD, SEM–EDS, and XPS to confirm the presence of silver in biochars after adsorption and prove their efficiency for the successful mitigation of silver pollution.

XRD spectrum of silver-loaded biochar is shown in Fig. 2b. Four sharp peaks at 2θ of 26.07° (210), 30.03° (122), 38.06° (111), and 44.2° (200) were observed. All peaks can be attributed to the presence of crystalline silver nanoparticles [80], which were otherwise absent in the biochars before adsorption. The planes observed can be recognised as pure silver based on the face-centered cubic structure (JCPDS, file No. 04–0783). These findings demonstrate that the silver ions were reduced during adsorption and produced Ag NPs on the biochar surface.

The presence of silver particles and their oxidation state in biochar samples was further confirmed by XPS analysis. Figure 2d shows the results of XPS analysis for SCG biochar after Ag^+ adsorption, showing the electron binding energies of Ag $3d_{5/2}$ and Ag $3d_{3/2}$ orbitals. A separate table of XPS analysis can be found in supplementary data Table S10. For silver ions, Ag $3d_{5/2}$ and Ag $3d_{3/2}$ orbitals can be further divided into 368.56/369.34 and 374.54/375.29 eV, respectively [81]. The peaks at the binding energy of 368.56/369.34 eV can be attributed to the presence of Ag^+ in the biochar, while peaks at 374.54/375.29 eV can be ascribed to metallic Ag^0 [82]. According to Table S10, 34.60% and 6.54% of the atomic concentration of Ag^+ were reduced to metallic Ag^0 and Ag^{2+}, respectively. These findings confirmed the chemisorption phenomenon, which was revealed by the kinetic and isothermal studies of silver adsorption by SCG biochar.

Figure 4a–c illustrate the SEM images of SCG biochar produced at 500 °C before adsorption and show that biochar had a rough, rigid, uneven, and irregular cracked surface. Figure 4d–f show SEM images of biochar after silver adsorption. Significant changes can be seen in the biochar surface compared to the untreated biochar samples, showing the homogeneous distribution of silver particles as white spots on the biochar surface. These white spots are silver nanoparticles that were confirmed by SEM–EDS analysis [67]. Small and large white spots on the surface indicated silver particles less than 100 nm in diameter. Large white clusters are the agglomerates of Ag NPs, which might be produced after the surface reduction of silver ions (Ag^+) [78].

In addition, EDS mapping (shown in Fig. 4g) confirms the adsorption of silver by biochar, confirming the presence of 3.18 wt% silver on SCG biochar. Other major elements such as carbon, oxygen, and trace amounts of other elements, such as magnesium, were also found in the biochar. The biochar samples successfully demonstrated the adsorption of silver, suggesting that biochar could be an efficient adsorbent for silver removal from wastewater.

4 Mechanism of silver adsorption on biochar

The characterisation studies like FTIR and EDS analyses confirmed the presence of various types of functional groups such as –OH and –COOH and elements like Ca, K, Al, and Si. Moreover, XPS results confirmed the reduction of Ag ions to metallic Ag. Therefore, based on these analyses and speculations from previous studies, different mechanisms of

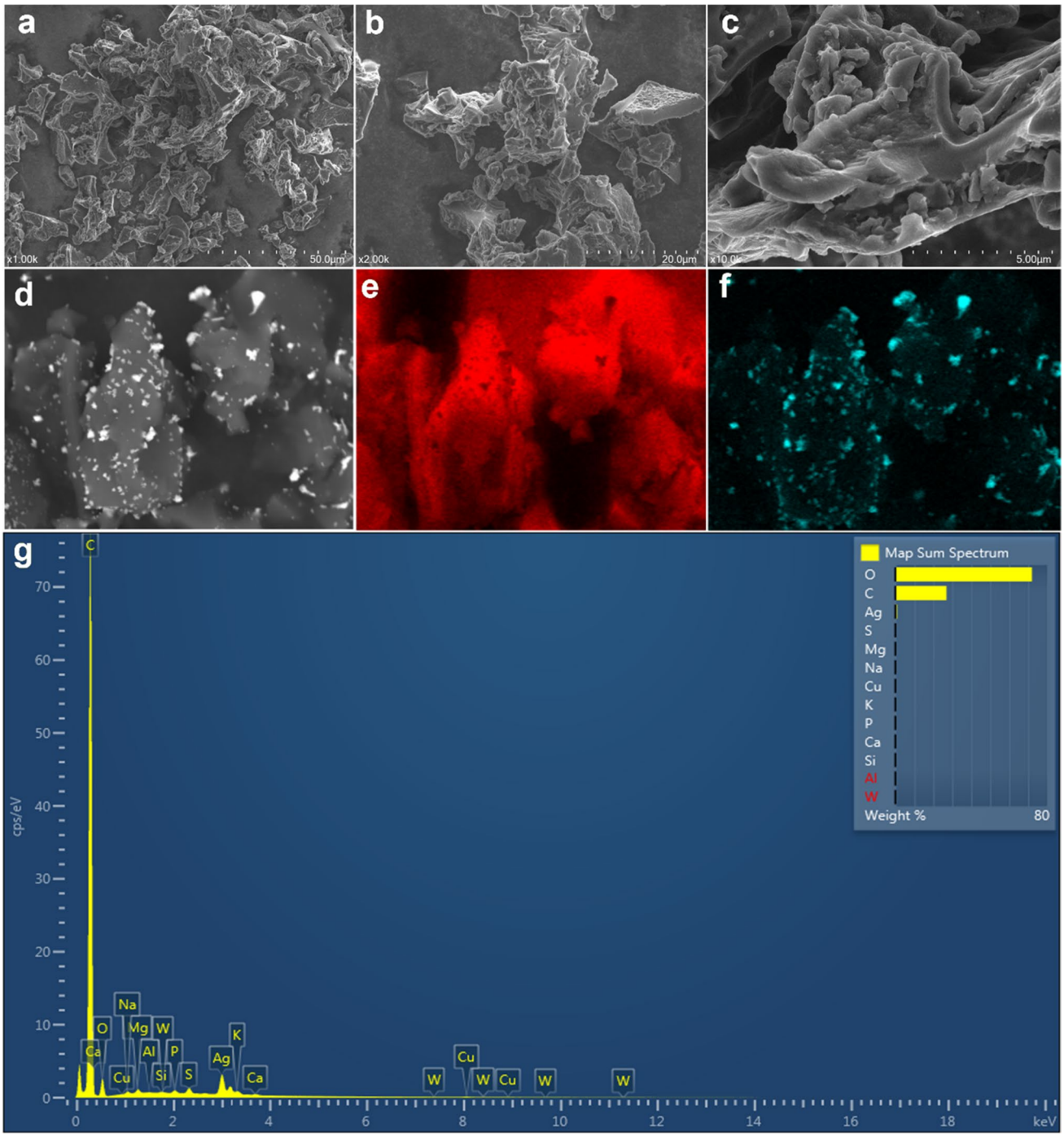

Fig. 4 **a**–**c** SEM images of SCG biochar produced at 500 °C before silver adsorption experiments; **d**–**f** SEM images of SCG biochar after silver adsorption; **d** backscattering image where the silver nanoparticles are white spots; **e** refers to the carbon distribution in the biochar; **f** refers to the silver distribution on the biochar; **g** EDS mapping spectra showing the elemental quantification in biochar after Ag adsorption

Ag adsorption on SCG biochar can be proposed. Figure 5 shows the possible mechanisms of Ag adsorption on SCG biochar. The most common Ag adsorption mechanism can be physical adsorption. SEM and BET analyses indicate the porous structure of the biochar; therefore, it can be predicted that Ag ions can be physically adsorbed to the biochar via the Van der Waals forces. Ag ions can be adsorbed on the surface of the biochar or can diffuse into the pores of the biochar. The strength of physical adsorption is generally considered weak and may depend on the surface area and pore

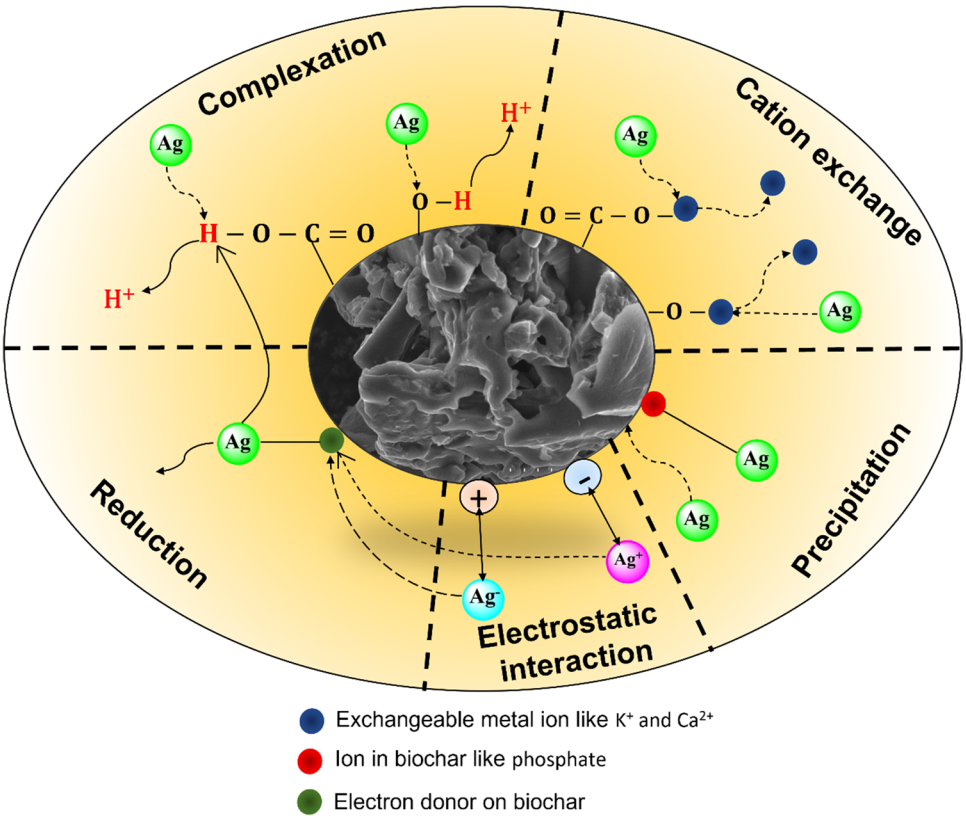

Fig. 5 Possible silver adsorption mechanisms on biochar. The main Ag adsorption mechanisms on biochar estimated in the study involve electrostatic interactions, physical adsorption, cation exchange, complexation, and reduction

volume. The BET analysis in our study suggests that the high temperature above 800 °C produced biochar with low surface area and pore volume, while 500 °C generated biochar with a maximum surface area of 40.10 m^2/g and pore volume of 0.019 cc/g, which suggests that the latter biochar would favour physical adsorption mechanism for the Ag removal. Physical adsorption of heavy metals on biochar has been demonstrated in previous studies. For instance, Zhang et al. (2019) demonstrated Pb removal from an aqueous solution using sludge-based biochar and revealed from isothermal and kinetics analyses that the main mechanism for Pb removal was physical adsorption rather than chemical adsorption [75].

The main mechanism for Ag removal that can be estimated from our analyses is electrostatic interactions between Ag species and surface-charged biochar. EDS analysis showed the presence of various elements which could be presented in positively or negatively charged forms and have the tendency to interact with oppositely charged Ag ions. The literature suggests that low pH offers a high concentration of H^+ in the solution, and thus the biochar surface groups combine with H^+, which reduces the negative charge, consequently resulting in the reduced adsorption capacity for heavy metal cations [27]. On the other hand, at the high pH of the aqueous solution, biochar surface groups lose protons, which increases the negative charge, and, subsequently, the adsorption capacity for heavy metal cations increases [27]. Since our study was conducted in high pH solution, the biochar is predicted to contain more negatively charged species, constructing electrostatic interactions with positively charged Ag ions and resulting in the enhanced adsorption capacity.

Another possible Ag removal mechanism may involve cation exchange. The functional groups on the biochar surface play an important role in the cation exchange mechanism. FTIR and EDS analyses confirm the presence of –COOH and elements like Ca, Na, and K. Thus, it can be predicted that Ca^{2+} and K^+ can be replaced on biochar with positively charged Ag ions like Ag^{2+} or Ag^+. The cation exchange of heavy metals on biochar is well known in the literature [83]. Complexation, which involves the formation of complex structures with specific metal–ligand interactions and precipitation that includes the formation of solids, is another known mechanism contributing to the removal of heavy metals from biochar [84]. XPS analysis confirmed the presence of metallic Ag species in the biochar, which suggests that the reduction process also took place during the Ag adsorption.

5 Conclusions

This study investigated the SCG biomass pyrolysis and the effect of pyrolysis temperature from 500 to 1000 °C on the properties of SCG biochar and their implication for silver adsorption from water solution. Results revealed that 10 °C/min was the optimum heating rate for the pyrolysis of SCGs. Py-GCMS and pyrolysis kinetic studies showed that SCG

biomass had a slightly different composition than lignocellulosic biomasses (Figures S2 and S3, Tables S4 and S5). Fluctuation of activation energy and higher molecular weight compounds demonstrate the complex decomposition behaviour of SCG biomass. In addition, Py-GCMS analysis opened the possibility of collecting bio-oil during pyrolysis to offset the biochar production cost. Biochar produced at 500 °C provided the maximum yield of 23.48% biochar, the highest surface area of 40.1 m^2/g, and pore volume of 0.019 cc/g. Also, the silver adsorption performance showed that the biochar produced at 500 °C achieved a maximum adsorption capacity of 49.0 mg/g with 99.9% silver removal efficiency. In contrast, biochars produced at 1000 °C achieved the lowest adsorption capacity of 23.6 mg/g with 48.1% silver removal efficiency. Low adsorption efficiency by biochars produced at higher temperatures could be attributed to their low surface area and pore volume and the smaller number of functional groups. SEM–EDS results showed an even distribution of silver on the biochar surface. XPS analysis confirmed the presence of metallic silver (Ag^0) on the biochar surface, indicating the partial chemical transformation of silver ions during adsorption. The kinetic study validated that silver adsorption by SCG biochar supported the pseudo-second-order model, which revealed the presence of chemisorption. Additionally, isothermal analysis established that the batch process of silver removal was dominated by homogeneous monolayer adsorption. This study indicates that biochar production from SCGs can be used as an adsorbent that is a sustainable approach to mitigate silver pollution while avoiding the hazardous consequences of landfilling of SCGs. However, further studies are required to evaluate the impact of the activation of SCG biochar on the silver adsorption performance with co-existing pollutants. A pilot scale using a continuous adsorption column is required to better understand the capacity to handle large volumes of wastewater contaminated with silver species.

Supplementary Information The online version contains supplementary material available at https://doi.org/10.1007/s13399-022-03491-0.

Author contribution Md Anwarul Islam and Elsa Antunes proposed the research and designed the experiments. Md Anwarul Islam and Tewodros Kassa Dada conducted the experiments. Md Anwarul Islam, Tewodros Kassa Dada, Mst Irin Parvin, and Ravinder Kumar analysed experimental results and reviewed and edited the manuscript. Elsa Antunes supervised, reviewed, and edited the manuscript. All authors read the manuscript and approved it for publication.

Funding Open Access funding enabled and organized by CAUL and its Member Institutions

Data availability All data are available upon request.

Declarations

Ethics approval and consent to participate Not applicable.

Consent for publication All authors agreed on the publication of this research work.

Competing interests The authors declare no competing interests.

References

1. Jones ER et al (2021) Country-level and gridded estimates of wastewater production, collection, treatment and reuse. Earth System Sci Data 13(2):237–254
2. Islam MA et al (2022) Silver ions and silver nanoparticles removal by coffee derived biochar using a continuous fixed-bed adsorption column. J Water Process Eng 48:102935
3. Mahmoud ME, El-Bahy SM, Elweshahy SM (2021) Decorated Mn-ferrite nanoparticle@ Zn–Al layered double hydroxide@ Cellulose@ activated biochar nanocomposite for efficient remediation of methylene blue and mercury (II). Biores Technol 342:126029
4. Agoro MA et al (2020) Heavy metals in wastewater and sewage sludge from selected municipal treatment plants in eastern cape province, south africa. Water 12(10):2746
5. Mahmoud, M.E., A.M. El-Ghanam, and S.R. Saad, Sequential removal of chromium (VI) and prednisolone by nanobiochar-enriched-diamine derivative. Biomass Conversion and Biorefinery, 2022: p. 1–20.
6. Mahmoud ME et al (2021) Doping starch-gelatin mixed hydrogels with magnetic spinel ferrite@ biochar@ molybdenum oxide as a highly efficient nanocomposite for removal of lead (II) ions. J Environ Chem Eng 9(6):106682
7. Yan N, Wang W-X (2021) Novel imaging of silver nanoparticle uptake by a unicellular alga and trophic transfer to Daphnia magna. Environ Sci Technol 55(8):5143–5151
8. Mahmoud ME et al (2021) Novel immobilized fibrous natural cotton on Corchorus olitorius stalks biochar@ diethylenetriamine@ feroxyhyte@ diethylenetriamine composite for coagulative removal of silver quantum dots (Ag-QDs) from water. Cellulose 28(18):11397–11416
9. Bhuyar P et al (2020) Synthesis of silver nanoparticles using marine macroalgae Padina sp. and its antibacterial activity towards pathogenic bacteria. Beni-Suef Univ J Basic Appl Sci 9(1):1–15.
10. Bhuyar P et al (2021) Removal of nitrogen and phosphorus from agro-industrial wastewater by using microalgae collected from coastal region of peninsular Malaysia. Afr J Biol Sci 3(1):58–66
11. Mahmoud ME et al (2022) Adsorption behavior of silver quantum dots by a novel super magnetic CoFe2O4-biochar-polymeric nanocomposite. J Colloid Interface Sci 606:1597–1608
12. Zhang W et al (2019) Fate and toxicity of silver nanoparticles in freshwater from laboratory to realistic environments: a review. Environ Sci Pollut Res 26(8):7390–7404

13. Antunes E et al (2017) Silver removal from aqueous solution by biochar produced from biosolids via microwave pyrolysis. J Environ Manage 203(Pt 1):264–272
14. Silva-Medeiros FV et al (2016) Kinetics and thermodynamics studies of silver ions adsorption onto coconut shell activated carbon. Environ Technol 37(24):3087–3093
15. Cantuaria ML et al (2016) Adsorption of silver from aqueous solution onto pre-treated bentonite clay: complete batch system evaluation. J Clean Prod 112:1112–1121
16. Zhang M, Helleur R, Zhang Y (2015) Ion-imprinted chitosan gel beads for selective adsorption of Ag+ from aqueous solutions. Carbohyd Polym 130:206–212
17. Whangchai K et al (2021) Biomass generation and biodiesel production from macroalgae grown in the irrigation canal wastewater. Water Sci Technol 84(10–11):2695–2702
18. Saman N et al (2015) Silver adsorption enhancement from aqueous and photographic waste solutions by mercerized coconut fiber. Sep Sci Technol 50(7):937–946
19. Chu C-Y et al (2021) High performance of biohydrogen production in packed-filter bioreactor via optimizing packed-filter position. Int J Environ Res Public Health 18(14):7462
20. Wajima T (2016) Synthesis of zeolitic material from green tuff stone cake and its adsorption properties of silver (I) from aqueous solution. Microporous Mesoporous Mater 233:154–162
21. Liu Y et al (2019) Understanding the high adsorption-reduction performance of triethanolamine modified graphene oxide for silver ions. Colloids Surf, A 567:96–103
22. Mahmoud ME, Mohamed AK, Salam MA (2021) Self-decoration of N-doped graphene oxide 3-D hydrogel onto magnetic shrimp shell biochar for enhanced removal of hexavalent chromium. J Hazard Mater 408:124951
23. Mahmoud ME, Abou-Ali SA, Elweshahy SM (2021) Efficient and ultrafast removal of Cd (II) and Sm (III) from water by leaves of Cynara scolymus derived biochar. Mater Res Bull 141:111334
24. Islam MA, Jacob MV, Antunes E (2021) A critical review on silver nanoparticles: from synthesis and applications to its mitigation through low-cost adsorption by biochar. J Environ Manage 281:111918
25. Yao Y et al (2015) Engineered biochar from biofuel residue: characterization and its silver removal potential. ACS Appl Mater Interfaces 7(19):10634–10640
26. Dong X, Ma LQ, Li Y (2011) Characteristics and mechanisms of hexavalent chromium removal by biochar from sugar beet tailing. J Hazard Mater 190(1–3):909–915
27. Qiu B et al (2021) Biochar as a low-cost adsorbent for aqueous heavy metal removal: a review. J Anal Appl Pyrolysis 155.
28. Armstrong DL et al (2016) Temporal trends of perfluoroalkyl substances in limed biosolids from a large municipal water resource recovery facility. J Environ Manage 165:88–95
29. Li X, Strezov V, Kan T (2014) Energy recovery potential analysis of spent coffee grounds pyrolysis products. J Anal Appl Pyrol 110:79–87
30. Tala W, Chantara S (2019) Use of spent coffee ground biochar as ambient PAHs sorbent and novel extraction method for GC-MS analysis. Environ Sci Pollut Res 26(13):13025–13040
31. Zhang X et al (2020) Characterization and sulfonamide antibiotics adsorption capacity of spent coffee grounds based biochar and hydrochar. Sci Total Environ 716:137015–137015
32. Jayakumar S et al (2021) Effects of light intensity and nutrients on the lipid content of marine microalga (diatom) Amphiprora sp. for promising biodiesel production. Sci Total Environ 768:145471
33. Ma'arof NANB et al (2021) Exploitation of cost-effective renewable heterogeneous base catalyst from banana (Musa paradisiaca) peel for effective methyl ester production from soybean oil. Appl Nanosci 2021:1–12.
34. Jeon C (2017) Adsorption of silver ions from industrial wastewater using waste coffee grounds. Korean J Chem Eng 34(2):384–391
35. Antunes E et al (2017) Biochar produced from biosolids using a single-mode microwave: characterisation and its potential for phosphorus removal. J Environ Manage 196:119–126
36. Bardestani R, Patience GS, Kaliaguine S (2019) Experimental methods in chemical engineering: specific surface area and pore size distribution measurements—BET, BJH, and DFT. Can J Chem Eng 97(11):2781–2791
37. Meng F et al (2019) The contribution of oxygen-containing functional groups to the gas-phase adsorption of volatile organic compounds with different polarities onto lignin-derived activated carbon fibers. Environ Sci Pollut Res 26(7):7195–7204
38. Romero Millán LM, Sierra Vargas FE, Nzihou A (2017) Kinetic analysis of tropical lignocellulosic agrowaste pyrolysis. BioEnergy Res 10(3):832–845.
39. Kabir G, Hameed B (2017) Recent progress on catalytic pyrolysis of lignocellulosic biomass to high-grade bio-oil and biochemicals. Renew Sustain Energy Rev 70:945–967
40. Kumar R et al (2019) Bio-oil upgrading with catalytic pyrolysis of biomass using copper/zeolite-Nickel/zeolite and Copper-Nickel/zeolite catalysts. Bioresour Technol 279:404–409
41. Campos-Vega R et al (2015) Spent coffee grounds: a review on current research and future prospects. Trends Food Sci Technol 45(1):24–36
42. Rodriguez, C. and G. Gordillo, Adiabatic gasification and pyrolysis of coffee husk using air-steam for partial oxidation. Journal of Combustion, 2011.
43. Milosavljevic I, Suuberg EM (1995) Cellulose thermal decomposition kinetics: global mass loss kinetics. Ind Eng Chem Res 34(4):1081–1091
44. Gonnella G et al (2022) Thermal analysis and kinetic modeling of pyrolysis and oxidation of hydrochars. Energies 15(3):950
45. Rijo B et al (2021) Catalyzed pyrolysis of coffee and tea wastes. Energy 235:121252
46. Mishra G, Kumar J, Bhaskar T (2015) Kinetic studies on the pyrolysis of pinewood. Biores Technol 182:282–288
47. Lee XJ et al (2021) Solid biofuel production from spent coffee ground wastes: process optimisation, characterisation and kinetic studies. Fuel 292:120309
48. Burnham AK, Zhou X, Broadbelt LJ (2015) Critical review of the global chemical kinetics of cellulose thermal decomposition. Energy Fuels 29(5):2906–2918
49. He Q et al (2019) Effect of torrefaction on pinewood pyrolysis kinetics and thermal behavior using thermogravimetric analysis. Biores Technol 280:104–111
50. Yuan X et al (2017) Cattle manure pyrolysis process: kinetic and thermodynamic analysis with isoconversional methods. Renewable Energy 107:489–496
51. Xu Y, Chen B (2013) Investigation of thermodynamic parameters in the pyrolysis conversion of biomass and manure to biochars using thermogravimetric analysis. Biores Technol 146:485–493
52. Pattanayak S et al (2021) Experimental investigation on pyrolysis kinetics, reaction mechanisms and thermodynamic parameters of biomass and tar in N2 atmosphere. Sustain Energy Technol Assess 48:101632
53. Loy ACM et al (2018) Thermogravimetric kinetic modelling of in-situ catalytic pyrolytic conversion of rice husk to bioenergy using rice hull ash catalyst. Biores Technol 261:213–222
54. Fu J et al (2022) Torrefaction, temperature, and heating rate dependencies of pyrolysis of coffee grounds: its performances, bio-oils, and emissions. Biores Technol 345:126346
55. Mallick D et al (2018) Discernment of synergism in pyrolysis of biomass blends using thermogravimetric analysis. Biores Technol 261:294–305

56. He J et al (2019) Effect of temperature on heavy metal(loid) deportment during pyrolysis of Avicennia marina biomass obtained from phytoremediation. Bioresour Technol 278:214–222
57. Kan T, Strezov V, Evans TJ (2016) Lignocellulosic biomass pyrolysis: a review of product properties and effects of pyrolysis parameters. Renew Sustain Energy Rev 57:1126–1140
58. Ktori R, Kamaterou P, Zabaniotou A (2018) Spent coffee grounds valorization through pyrolysis for energy and materials production in the concept of circular economy. Materials Today: Proceedings 5(14):27582–27588
59. Lee Y et al (2013) Comparison of biochar properties from biomass residues produced by slow pyrolysis at 500 C. Biores Technol 148:196–201
60. Shin J et al (2020) Effects of physicochemical properties of biochar derived from spent coffee grounds and commercial activated carbon on adsorption behavior and mechanisms of strontium ions (Sr2+). Environ Sci Pollut Res Int
61. Chwastowski J, Bradło D, Żukowski W (2020) Adsorption of cadmium, manganese and lead ions from aqueous solutions using spent coffee grounds and biochar produced by its pyrolysis in the fluidized bed reactor. Materials 13(12):2782
62. Sing K (2001) The use of nitrogen adsorption for the characterisation of porous materials. Colloids Surf, A 187:3–9
63. Ambroz F et al (2018) Evaluation of the BET theory for the characterization of meso and microporous MOFs. Small Methods 2(11):1800173
64. Zhao B et al (2018) Effect of pyrolysis temperature, heating rate, and residence time on rapeseed stem derived biochar. J Clean Prod 174:977–987
65. Cha JS et al (2016) Production and utilization of biochar: a review. J Ind Eng Chem 40:1–15
66. Jagdale P et al (2019) Waste coffee ground biochar: a material for humidity sensors. Sensors (Basel, Switzerland) 19(4):801
67. Gicheva G, Yordanov G (2013) Removal of citrate-coated silver nanoparticles from aqueous dispersions by using activated carbon. Colloids Surf, A 431:51–59
68. Zhang L et al (2020) Preparation of biochar by mango peel and its adsorption characteristics of Cd (II) in solution. RSC Adv 10(59):35878–35888
69. Shaikh WA et al (2022) Biochar-based nanocomposite from waste tea leaf for toxic dye removal: from facile fabrication to functional fitness. Chemosphere 291:132788
70. Zhao T et al (2018) Facile low-temperature one-step synthesis of pomelo peel biochar under air atmosphere and its adsorption behaviors for Ag (I) and Pb (II). Sci Total Environ 640:73–79
71. Tomczyk A, Sokołowska Z, Boguta P (2020) Biomass type effect on biochar surface characteristic and adsorption capacity relative to silver and copper. Fuel (Guildford) 278:118168
72. Naga Babu A et al (2021) Mathematical investigation into the sequential adsorption of silver ions and brilliant green dye using biochar derived from Gracilaria Rhodophyta algae. Biomass Convers Biorefinery 2021:1–20.
73. Peng H et al (2021) Reduction of silver ions to silver nanoparticles by biomass and biochar: mechanisms and critical factors. Sci Total Environ 779:146326
74. Hussain N et al (2020) Cadmium (II) removal from aqueous solution using magnetic spent coffee ground biochar: kinetics, isotherm and thermodynamic adsorption. Mater Res Express 7(8):085503
75. Zhang J et al (2019) Sludge-based biochar activation to enhance Pb(II) adsorption. Fuel 252:101–108
76. Kılıç M et al (2013) Adsorption of heavy metal ions from aqueous solutions by bio-char, a by-product of pyrolysis. Appl Surf Sci 283:856–862
77. Hashem A et al (2020) Non-linear adsorption characteristics of modified pine wood sawdust optimised for adsorption of Cd (II) from aqueous systems. J Environ Chem Eng 8(4):103966
78. Zhou Y et al (2014) Biochar-supported zerovalent iron reclaims silver from aqueous solution to form antimicrobial nanocomposite. Chemosphere 117:801–805
79. Kołodyńska D et al (2012) Kinetic and adsorptive characterization of biochar in metal ions removal. Chem Eng J 197:295–305
80. Anandalakshmi K, Venugobal J, Ramasamy V (2016) Characterization of silver nanoparticles by green synthesis method using Pedalium murex leaf extract and their antibacterial activity. Appl Nanosci 6(3):399–408
81. Khan NA et al (2006) Alumina supported model Pd–Ag catalysts: a combined STM, XPS TPD and IRAS study. Surface Sci 600(9):1849–1853
82. Ren M et al (2018) Titanium phosphate nanoplates modified with AgBr@Ag nanoparticles: a novel heterostructured photocatalyst with significantly enhanced visible light responsive activity. Front Chem 6:489
83. Ambaye TG et al (2020) Mechanisms and adsorption capacities of biochar for the removal of organic and inorganic pollutants from industrial wastewater. Int J Environ Sci Technol 18(10):3273–3294
84. Komkiene J, Baltrenaite E (2015) Biochar as adsorbent for removal of heavy metal ions [cadmium(II), copper(II), lead(II), zinc(II)] from aqueous phase. Int J Environ Sci Technol 13(2):471–482